Numerical Simulation Study of Damage-Front Redistribution under Continuous and Inert-Stemming Decked Charging in Near-Seam Open-Pit Blasting

Qichong Huang[1], Jianlong Wang[1,*], Qiang Zhao[1], Wenlong Zhao[1], Gele Aori[1], Zuoming Yin[1], Han Li[2], Lei Chi[1]

[1]North Blasting Technology Co., Ltd., Beijing, 100097, China
[2]Anhui Jiangnan Chemical Industry Co., Ltd., Hefei, 230088, China
*Corresponding author: jlwang98@163.com

Abstract. In near-seam benches of open-pit coal mines, only a narrow rock buffer may remain between the borehole bottom and the coal-seam roof. Bottom stemming and inert-stemming decked charging are used in field practice to limit coal loss and dilution, but the coal-side response is controlled by the local geometry. Unlike studies that focus mainly on air decks or decoupled charges, this work examines a fully filled inert-stemming interdeck used in coal-protection blasting. LS-DYNA was used to analyse a field-motivated near-seam condition from the Obo Tologoi open-pit coal mine, Mongolia. Continuous charging and inert-stemming decked charging were compared for 1.0 m and 0.5 m rock covers. The JH2 damage variable was exported as History Variable #2 and evaluated near 1.0 ms, when the early damage field was formed and the geometry remained comparable. No direct coal damage was identified at this state. A damage-front distance from the coal-seam roof was therefore used to represent the remaining intact buffer. For the 1.0 m cover, the distance was 0.94 m in the continuous case and 0.06 m in the decked case. For the 0.5 m cover, the corresponding values were 0.06 m and 0.44 m. The σ_{yy} histories support this interpretation: the C_0/R_0 peak-stress ratio changed from 0.73 in A2-1.0 to 0.20 in A4-0.5. The results indicate that decked charging redistributes the damage field rather than reducing damage in a uniform way. Its coal-side effect depends on the lower charge position, the coal-rock interface, and the remaining cover thickness, and should be calibrated before direct field use.

Keywords: near-seam blasting; open-pit coal mine; decked charging; coal-rock interface; damage front; LS-DYNA

1 Introduction

Near-seam blasting is a recurrent control problem in open-pit coal mining. In some benches, the borehole bottom can approach the coal-seam roof because the seam position is inferred during drilling or from limited exposure. The design must fragment the overlying rock while keeping a usable intact buffer above the coal seam. When the

© The Author(s) 2026
H. Wu et al. (eds.), *Proceedings of the 2026 3rd International Conference on Civil Engineering Structures and Concrete Materials (CESCM 2026)*, Advances in Engineering Research 312,
https://doi.org/10.2991/978-94-6239-865-8_6

damage front advances toward the roof, coal loss, dilution, and roof disturbance become more likely [1-3].

The issue is not controlled by charge quantity alone. Published open-pit blasting studies show that bench geometry, coal occurrence, and local geology can change the required blasting response [4-6]. In field operations, bottom stemming, lower charge reduction, or decked charging are often adopted when drilling cuttings indicate a near-seam condition. At the Obo Tologoi open-pit coal mine in South Gobi, Mongolia, bottom stemming and decked charging are used for coal protection. The practical question is therefore not simply whether a deck is present. It is whether this layout reduces coal-side damage or mainly shifts the damage field near the coal-rock interface.

Blast damage is commonly linked to stress-wave loading, gas pressure, and local fracture growth, with the balance between these processes controlled by geometry and confinement [7-10]. Studies on charge structure also show that air decking, cavity charges, decoupled charges, and stemming design affect borehole-wall pressure, loading duration, and fracture growth [11-18]. These findings suggest that modifying the charge column can change where damage develops around a borehole.

Previous work can be grouped into related but different streams. Studies on charge-structure optimization, air-decking, cavity charges, decoupled charges, and stemming design mainly show how the charge column changes borehole loading and fracture growth [11-18]. Studies on layered coal-rock systems focus on vibration transmission, interface response, or damage accumulation across the coal-rock boundary [19-23]. These streams support the present problem but do not fully address a field condition in which a fully filled inert-stemming interdeck is used above a thin rock buffer between the borehole bottom and the coal-seam roof. The specific gap is therefore a controlled comparison of continuous and inert-stemming decked charging under matched near-seam boundaries, with the damage-front distance from the coal-seam roof used as the main response index.

This study addresses that gap using LS-DYNA. The contribution is threefold. First, homogeneous-rock cases are used to isolate the baseline damage redistribution caused by the inert interdeck. Second, near-seam cases quantify the minimum distance between the damage front and the coal-seam roof under 1.0 m and 0.5 m cover conditions. Third, paired σ_{yy} histories at rock-cover and coal-side monitoring points are used to interpret stress transfer across the coal-rock interface. The study does not assume that decked charging is always protective. It examines how charge structure, lower charge position, interface response, and remaining rock cover jointly control early damage-front development.

2 Numerical Model and Methods

2.1 Engineering Problem and Modelling Scope

The model was built from a near-seam blasting condition at the Obo Tologoi open-pit coal mine in South Gobi, Mongolia. During drilling, coal cuttings may show that the

borehole bottom is close to the coal-seam roof. In that situation, the blast must break the overlying rock while leaving an intact buffer above the seam.

The numerical model was used to interpret that engineering response. It was not intended to reproduce a full production blast or predict absolute coal loss. The comparison focuses on how continuous charging and inert-stemming decked charging change the early damage-front position near the coal-rock interface. The remaining intact buffer is therefore the main evaluation target, rather than final muckpile fragmentation or absolute coal loss. The two-dimensional plane-strain assumption was adopted to keep this comparison controlled. It should be read as a screening model, not as a complete representation of radial cracking, burden relief, stemming plug motion, or bench-scale fracture development. Within this common framework, the calculated distances are used to rank charge layouts and interpret stress-transfer trends, not to set final field damage limits.

2.2 Model Geometry and Near-Seam Configuration

A two-dimensional plane-strain model was built in LS-DYNA (Figure 1). The model represents a vertical borehole in an upper rock mass overlying a coal seam. The borehole axis is placed at the model centre. The coal seam is represented as a lower stratum, and the coal-seam roof is used as the reference boundary for damage-front measurement. The model domain was 20 m wide and 22 m high. The coal seam occupied the lower 6 m of the model. The borehole was 15 m deep and had a diameter of 165 mm. In the main 1.0 m cover cases, the borehole bottom was located 1.0 m above the coal-seam roof. Because all cases use the same plane-strain simplification, the results are interpreted as relative changes in early damage-front position rather than a full three-dimensional crack pattern around a finite borehole.

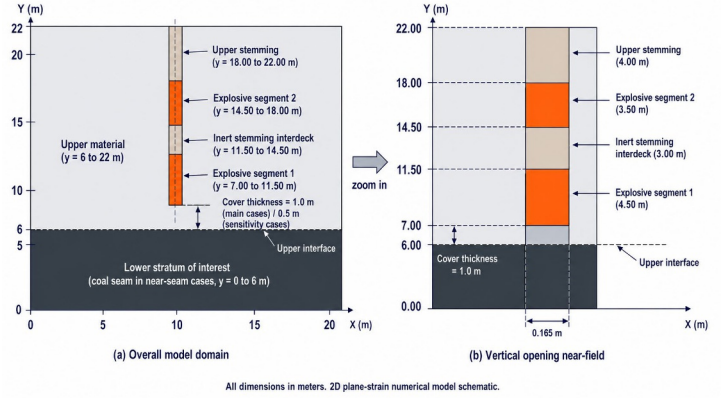


Fig. 1. Numerical model and charge-structure schematic. The schematic shows the two-dimensional near-seam model, the coal-seam roof, the rock-cover thickness, and the continuous and inert-stemming decked charge configurations used in the simulation cases.

Two near-seam cover conditions were considered. The main condition used a 1.0 m rock cover between the borehole bottom and the coal-seam roof. A 0.5 m cover was

used as a severe near-seam sensitivity condition. The two cover thicknesses probe whether a thinner intact buffer increases the damage-front sensitivity to charge structure and interface effects.

The homogeneous-rock cases remove the coal seam and provide baseline damage patterns. They are used to separate the influence of charge structure from the influence of the coal-rock interface.

2.3 Material Models and Fluid-Solid Coupling

Rock and coal were described by the Johnson-Holmquist ceramic damage model (JH2), which is commonly used to represent dynamic damage evolution in brittle geomaterials under high-rate loading [24-26]. The explosive was represented by a high-explosive burn model and a Jones-Wilkins-Lee equation of state. The stemming sections were treated as inert solid filler sections, so the decked configuration in this study should not be interpreted as an air-decked charge.

The explosive products and air domain were treated with an ALE description. Rock, coal, and stemming were treated with a Lagrangian description. ALE-Lagrange coupling transmitted the blast loading from detonation products to the surrounding solid media. The solver output was used to confirm the keyword interpretation of the JH2 material cards and numerical control settings.

Representative material settings are summarized in Table 1. Table 2 lists the comparison variables and fixed modelling controls that define the evidence chain.

Table 1. Representative material settings used in the numerical model.

Material	Constitutive / EOS model	Density (kg/m^3)	Key stiffness parameter	Key strength or loading parameter
Rock mass	JH2 damage model	2575	G = 7.84 GPa	T = 5.60 MPa; HEL = 1.98 GPa
Coal seam	JH2 damage model	1400	G = 1.14 GPa	T = 3.00 MPa; HEL = 1.50 GPa
Inert stemming	Plastic-kinematic model	1300	E = 0.50 GPa; nu = 0.35	Yield stress = 1.00 MPa
Explosive	High-explosive burn model with JWL EOS	1150	Detonation velocity = 4300 m/s	CJ pressure = 3.43 GPa

Note: The table reports representative parameters needed to compare material roles. Full JH2, plastic-kinematic, and JWL constants are defined in the LS-DYNA keyword files.

Table 2. Key comparison variables and fixed modelling controls.

Category	Treatment in the present comparison	Reason for inclusion
Charge structure	Continuous charging in A1/A2; inert-stemming decked charging in A3/A4	Tests whether the interdeck redistributes the damage field.
Near-seam boundary	No coal seam in A1/A3; 1.0 m and 0.5 m rock cover in A2/A4	Separates charge-structure effects from coal-rock interface effects.
Active explosive amount	Matched between paired continuous and decked cases	Keeps the comparison focused on spatial distribution rather than total charge.
Post-processing state	JH2 damage variable from History Variable #2; fixed D = 0-1 scale; comparison near 1.0 ms	Maintains cross-case visual and quantitative consistency.

Note: Detailed material constants are defined in the LS-DYNA keyword files and were checked through solver output. The main manuscript emphasizes the variables that control the comparison logic.

2.4 Simulation Cases

Six cases were used to build the evidence chain. A1 is a continuous charge in homogeneous rock. A3 is an inert-stemming decked charge in homogeneous rock. These two cases provide baseline damage fields without a coal-rock interface.

A2 and A4 are the near-seam cases. A2 uses continuous charging, and A4 uses inert-stemming decked charging. A2-1.0 and A4-1.0 use a 1.0 m cover. A2-0.5 and A4-0.5 use a 0.5 m cover. The total charge amount is kept consistent between the continuous and decked cases, while the charge structure is changed. The case design is summarized in Table 3.

The two charge layouts are compared schematically in Figure 2. The continuous-charge case uses one active explosive section, whereas the decked-charge case divides the same active length into lower and upper explosive segments separated by inert stemming. This schematic clarifies that the comparison focuses on the vertical distribution of explosive sections along the borehole axis.

The case matrix was kept deliberately narrow. It tests a field-motivated mechanism rather than an optimized charge-structure design. Bottom stemming length, interdeck length, air decking, and multi-hole interaction are treated as follow-up variables.

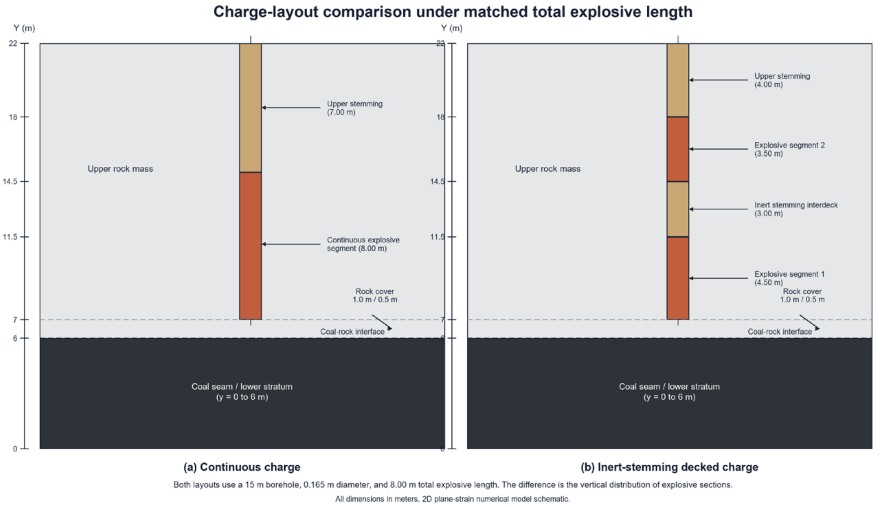


Fig. 2. Schematic comparison of continuous and inert-stemming decked charge layouts. (a) Continuous charge layout. (b) Inert-stemming decked charge layout. Both layouts use the same borehole diameter and matched total explosive length. The main difference is the vertical distribution of explosive sections along the borehole axis.

Table 3. Simulation cases and their role in the evidence chain.

Case	Coal seam / cover condition	Charge structure	Main comparison role
A1	Homogeneous rock; no coal seam	Continuous charge	Baseline continuous damage pattern.
A3	Homogeneous rock; no coal seam	Inert-stemming decked charge	Baseline damage redistribution caused by the interdeck.
A2-1.0	Coal seam; 1.0 m rock cover	Continuous charge	Near-seam reference under the main cover condition.
A4-1.0	Coal seam; 1.0 m rock cover	Inert-stemming decked charge	Tests decked-charge response under the main cover condition.
A2-0.5	Coal seam; 0.5 m rock cover	Continuous charge	Severe near-seam reference with reduced intact buffer.
A4-0.5	Coal seam; 0.5 m rock cover	Inert-stemming decked charge	Tests decked-charge response under the severe near-seam condition.

2.5 Damage Variable and Comparison State

In LS-PrePost, the JH2 damage variable was taken from History Variable #2. All cases used a fixed contour range of D = 0-1. ALE parts were hidden during damage-field post-processing. The viewpoint and colour scale were kept the same for cross-case comparison.

The main damage fields were compared near 1.0 ms. This time was selected as a damage-field comparison state because the main early damage pattern had formed while the model geometry remained suitable for comparison. Some later frames include severe element erosion or local geometry loss. Those frames are useful for understanding numerical failure, but they are not used as the main comparison state.

The comparison state is therefore not described as a final post-blast fragmentation state. This wording keeps the interpretation limited to early damage-front development.

2.6 Damage-front Distance Metric

At the selected comparison state, direct coal-seam damage was not detected in the four near-seam cases. Coal damage depth and damage width were therefore not sensitive enough to distinguish the cases. A damage-front distance metric was introduced to describe the remaining intact rock buffer above the coal-seam roof.

For each case, damaged elements above the coal-seam roof were screened using two thresholds, $D > 0.5$ and $D > 0.2$. The closest damaged point to the coal-seam roof was identified for each threshold. The vertical distance between this point and the coal-seam roof was defined as the damage-front distance. A larger distance indicates that the damage front remains farther from the coal seam at the comparison state.

This metric is a numerical screening index. It is not a direct field design criterion without calibration. Field application would require drilling records, exposed roof observations, coal loss, dilution, and vibration or stress monitoring.

2.7 Stress-Wave Monitoring and Curve Processing

Stress histories were extracted to support the interpretation of damage-front redistribution. The monitoring elements were selected by physical location and then matched to the nearest solid element in each case.

Two monitoring positions were used. R_0 was placed in the rock cover below the borehole bottom, and C_0 was placed below the coal-seam roof. R_0 represents the stress response before the wave reaches the coal-roof zone. C_0 represents the response after transmission into the seam. The vertical stress component σ_{yy}, exported as LS-DYNA SYY, was used because the analysis focuses on downward wave transfer from the borehole bottom to the coal seam.

The stress histories were described using the main compressive peak, any tensile peak, arrival time, and the C_0/R_0 peak ratio. These quantities provide mechanism evidence to be read together with the damage maps and damage-front metric. For A4,

only the available exported time window is interpreted; the late-time waveform is not discussed.

3 Results and Discussion

3.1 Baseline Damage-Field Pattern Under Continuous Charging

In A1, continuous charging produced the reference damage field in homogeneous rock (Figure 3a). Damage developed around the charge column and remained axially connected. This response gives the baseline loading and damage pattern around the borehole when no coal-rock interface is present.

A1 is not a coal-protection case. It is used as a homogeneous-rock reference, so the charge-structure effect can be separated from the coal-rock interface effect in the later comparisons.

3.2 Damage-Field Redistribution Induced by Inert-Stemming Decked Charging

A3 shows that the inert-stemming interdeck disrupts the spatial continuity of damage in homogeneous rock (Figure 3b). This behaviour agrees with studies showing that charge discontinuity, air decking, cavity structures, decoupling, and stemming design can alter borehole loading and fracture growth [11-18]. Relative to A1, the damage field splits into upper and lower local zones. The interdeck therefore acts mainly by redistributing damage, rather than by reducing it in a simple overall manner.

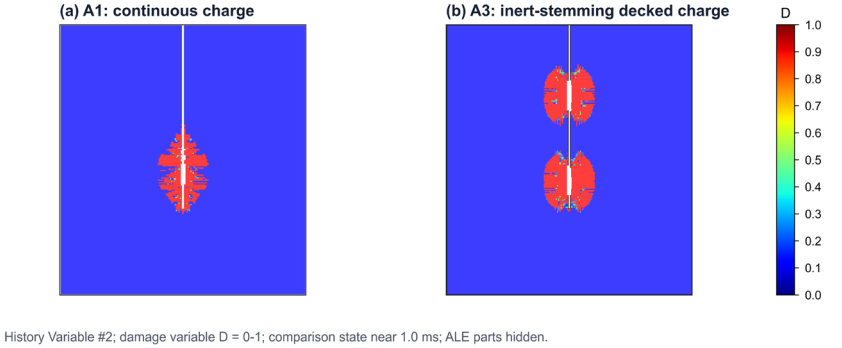


Fig. 3. Baseline damage fields in homogeneous rock under continuous and inert-stemming decked charging. (a) Continuous charge in homogeneous rock (A1). (b) Inert-stemming decked charge in homogeneous rock (A3). The JH2 damage variable was extracted as History Variable #2, and the contour range was fixed at D = 0-1. Continuous charging forms a connected damage zone along the charge column. Inert-stemming decked charging divides the damage field into upper and lower local regions. This figure provides the baseline comparison and does not directly evaluate coal-seam protection.

The interdeck divides the continuous charge column into two active loading sections. The upper and lower explosive segments become separate damage centers. Because the inert interdeck does not apply explosive loading, damage around this section is weaker than around the charged segments.

This baseline result frames the near-seam interpretation. If decked charging redistributes damage in homogeneous rock, its coal-side effect should depend on the spacing between the lower charge segment and the coal-rock interface.

3.3 Damage-Front Response Under 1.0 m Rock Cover

Under the 1.0 m rock-cover condition, neither A2-1.0 nor A4-1.0 showed coal-seam elements with $D > 0.2$ or $D > 0.5$ (Figure 4a,b; Table 4). Coal-seam damage depth and width therefore both remained zero. These two indices could not distinguish the effect of continuous and decked charging at this comparison state.

The damage-front distance provided a more sensitive comparison (Figure 5). In A2-1.0, the nearest damage front remained about 0.94 m from the coal-seam roof for both damage thresholds. This result indicates that the main damage zone under continuous charging had not approached the coal-seam roof at the comparison state. Most of the 1.0 m rock cover remained intact.

A4-1.0 showed a different response. The damage-front distance was about 0.06 m for both thresholds. The lower local damage zone was therefore close to the coal-seam roof. This result shows that inert-stemming decked charging does not necessarily move the damage front away from the coal seam. The interdeck separates the charge column and divides the damage field into local zones, but the lower explosive segment can still control the damage front when it is positioned close to the coal-rock interface.

The 1.0 m cases therefore define an important boundary for interpretation. Decked charging should not be judged only by the presence of an inert interdeck. Its effect also depends on the spatial relation between the lower charge segment, the borehole bottom, the coal-seam roof, and the remaining rock cover.

3.4 Damage-front Response Under 0.5 m Rock Cover

When the rock cover decreased to 0.5 m, the continuous-charge case showed a damage front very close to the coal-seam roof (Figure 4c; Table 4). In A2-0.5, the damage-front distance was about 0.06 m for both damage thresholds. Although direct coal-seam damage was still absent, the intact buffer above the coal seam had been strongly reduced. This result shows why coal-seam damage depth alone is not sufficient for near-seam blasting assessment.

A4-0.5 showed a larger remaining buffer (Figure 4d; Figure 5). The damage-front distance was about 0.44 m for both thresholds. Compared with A2-0.5, the decked charge retained a thicker intact rock layer above the coal-seam roof. The damage map suggests that the inert interdeck weakened the continuity of downward damage development. The continuous damage tendency was replaced by more localized damage zones.

The 0.5 m cases support a conditional coal-side response. Under this severe near-seam condition, inert-stemming decked charging reduced downward damage-front penetration and retained a thicker intact buffer in the present model. This is consistent with the field rationale for using bottom stemming and decked charging in coal-protection blasting. It should still be treated as a relative numerical comparison, not as a direct field design criterion.

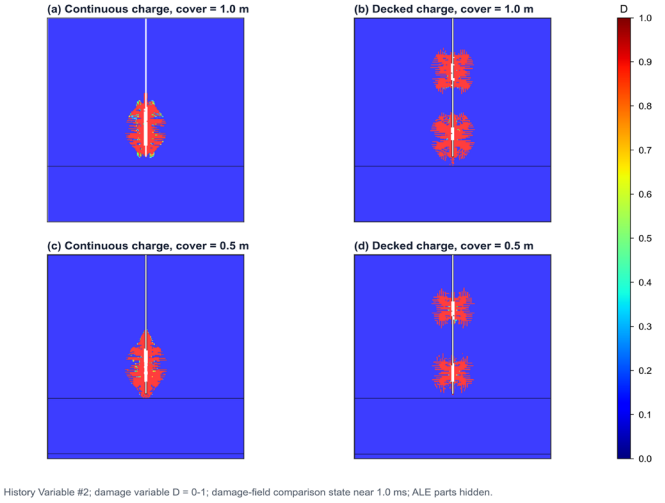


Fig. 4. Near-seam damage fields under continuous and inert-stemming decked charging at the damage-field comparison state. (a) Continuous charge with a 1.0 m rock cover (A2-1.0). (b) Inert-stemming decked charge with a 1.0 m rock cover (A4-1.0). (c) Continuous charge with a 0.5 m rock cover (A2-0.5). (d) Inert-stemming decked charge with a 0.5 m rock cover (A4-0.5). The JH2 damage variable was extracted through History Variable #2, and all panels use the same D = 0-1 scale. The coal-rock interface is shown as a horizontal line. The comparison indicates that decked charging changes the position and continuity of the lower damage front, and its coal-side effect depends on rock-cover thickness and lower charge position.

Table 4. Damage-front metrics extracted from the near-seam cases.

Case	Charge structure	Cover (m)	Comparison time (ms)	Direct coal damage at D > 0.2	Damage-front distance D > 0.5 / D > 0.2 (m)
A2-1.0	Continuous charge	1.00	1.01	Not detected	0.94 / 0.94
A4-1.0	Inert-stemming decked charge	1.00	1.05	Not detected	0.06 / 0.06
A2-0.5	Continuous charge	0.50	1.01	Not detected	0.06 / 0.06
A4-0.5	Inert-stemming decked charge	0.50	1.00	Not detected	0.44 / 0.44

Note: The damage-front distance is measured vertically from the coal-seam roof to the closest damaged element above the roof. A larger value indicates a thicker remaining intact rock buffer at the comparison state. Distances are mesh-based numerical measurements and are used for relative comparison.

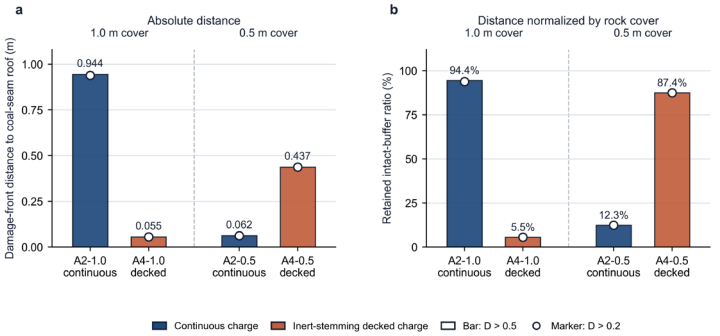


Fig. 5. Damage-front distance from the coal-seam roof at the comparison state near 1.0 ms. Bars denote D > 0.5, and open circles denote D > 0.2. A larger value indicates a thicker remaining intact rock buffer above the coal-seam roof.

3.5 Stress-Wave Evidence for Damage-Front Redistribution

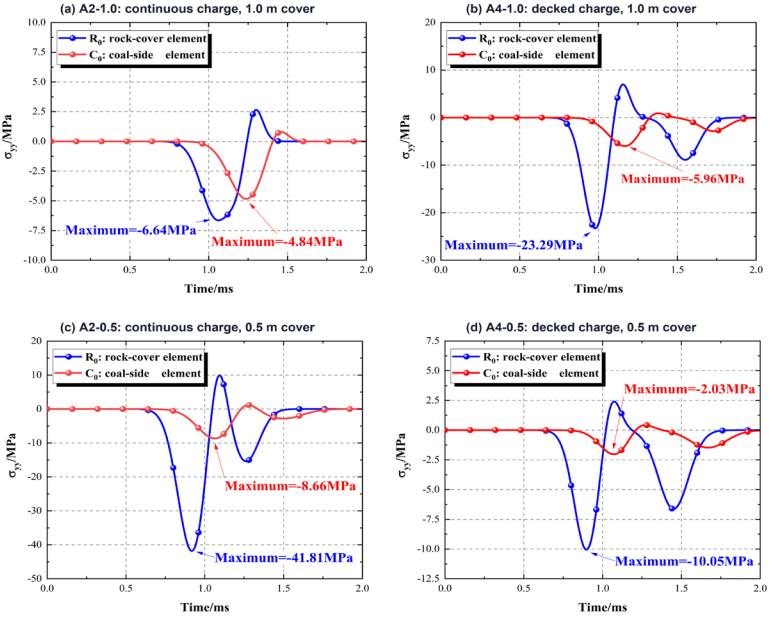


Fig. 6. σyy stress histories at R₀ and C₀ monitoring elements. (a) A2-1.0. (b) A4-1.0. (c) A2-0.5. (d) A4-0.5. R₀ is located in the rock cover below the borehole bottom, and C₀ is located below the coal-seam roof. The curves describe the vertical stress response used to interpret stress-wave transfer from the rock-cover zone to the coal-side monitoring point. Because each panel uses its own y-axis range for readability, cross-case comparison should be based on the listed peak values rather than visual curve height.

The σ_{yy} histories help connect charge structure, interface transfer, and damage-front position (Figure 6; Table 5). R_0 records the vertical stress response in the rock cover below the borehole bottom. C_0 records the response below the coal-seam roof. The C_0/R_0 compressive-peak ratio is used as a relative index of vertical stress-wave transfer across the near-seam zone.

For A2-1.0, the R_0 element recorded a compressive σ_{yy} peak of -6.64 MPa at 1.07 ms. The C_0 element recorded a lower compressive peak of -4.84 MPa at 1.22 ms. The C_0/R_0 ratio was 0.73. This response indicates a delayed and attenuated vertical stress wave after the wave moved from the rock-cover zone toward the coal-seam roof. The stress history is consistent with the damage map, in which the damage front remained far from the coal-seam roof at the comparison state.

For A2-0.5, the R_0 element recorded a stronger compressive peak of -41.81 MPa at 0.82 ms. The C_0 element recorded a lower compressive peak of -8.66 MPa at 1.03 ms. The C_0/R_0 ratio decreased to 0.21. The thinner rock cover therefore produced a stronger local response near the borehole-bottom side, but the transmitted response below the coal-seam roof was strongly reduced. This result is consistent with attenuation and interface-controlled transfer before the stress wave reached the coal-side monitoring point.

The decked cases show that the inert-stemming interdeck changes the location and intensity of the rock-cover response. A4-1.0 recorded R_0 and C_0 compressive peaks of -23.29 MPa and -5.98 MPa, and the C_0/R_0 ratio was 0.26. A4-0.5 recorded corresponding values of -10.05 MPa and -2.03 MPa, with a C_0/R_0 ratio of 0.20. These values show that the coal-side response remained lower than the rock-cover response in both decked cases, while the damage maps show that the lower local damage zone can move differently under different cover conditions.

Table 5. Characteristic σ_{yy} parameters extracted from paired R_0 and C_0 monitoring elements.

Case	Cover (m)	R_0 compressive peak (MPa)	C_0 compressive peak (MPa)	C_0/R_0 peak ratio	Interpretation
A2-1.0	1.00	-6.64	-4.84	0.73	Moderate attenuation from rock cover to coal side.
A4-1.0	1.00	-23.29	-5.98	0.26	Strong rock-cover response with lower transmitted coal-side response.
A2-0.5	0.50	-41.81	-8.66	0.21	Strong local response near the reduced rock cover.
A4-0.5	0.50	-10.05	-2.03	0.20	Lower coal-side peak under the severe near-seam condition.

Note: R_0 is the rock-cover monitoring element, and C_0 is the coal-side monitoring element. The values are based on the vertical stress component σ_{yy}, corresponding to LS-DYNA SYY. The ratio uses absolute compressive peak values. Each curve panel in Figure 6 uses an independent y-axis range; Table 5 should be used for quantitative cross-case comparison.

The damage maps and stress histories together point to a two-step process: the inert interdeck first divides the charge-induced damage field into local zones, and the coal-rock interface and remaining rock cover then govern how much of the vertical stress response is transmitted into the coal-side monitoring point. This explains why decked charging can retain a larger buffer in the 0.5 m case, but can also place a lower damage zone close to the roof in the 1.0 m case. The stress curves are used as mechanism evidence together with the damage-field and damage-front results, not as a standalone validation of final fragmentation.

3.6 Mechanism, Engineering Implications, and Limitations

The results indicate that inert-stemming decked charging acts through damage-field redistribution before it can be judged as protective or unfavorable. This point is the main distinction from a general statement that decked charging reduces damage. Prior studies on air-decking, cavity charges, decoupling, and stemming structure report that charge discontinuity can change borehole loading and fracture development [11-18]. In the present model, however, the interdeck is not an air gap. It is an inert stemming section that mechanically separates the active charge segments and maintains confinement. The relevant question is therefore where the lower local damage zone forms relative to the coal-seam roof.

The near-seam results show that this redistribution is boundary dependent. Under the 1.0 m cover condition, the A4-1.0 damage front was closer to the coal-seam roof than the A2-1.0 front. This means that a decked charge can concentrate the lower local damage zone near the roof if the lower charge segment is close to the interface. Under the 0.5 m cover condition, A4-0.5 retained a larger intact buffer than A2-0.5. The same charge concept can therefore produce different coal-side responses when the lower charge position and remaining rock cover change.

The coal-rock interface should be treated as an active part of the damage process, not as a passive boundary. Layered coal-rock systems can produce interface-controlled vibration and stress transfer [19-23]. In the simulations, the interface did not lead to direct coal damage at the comparison state, but it changed the remaining buffer above the coal-seam roof. This is why the damage-front distance is more useful than coal-seam damage depth for the present early comparison state.

In engineering practice, the results inform a cautious pre-design screening of near-seam layouts. When drilling indicates that the borehole bottom is close to the coal seam, the charge structure should be checked against the lower charge position, bottom stemming length, interdeck position, and remaining rock cover. The objective is not only to avoid damaged coal elements. It is to retain a measurable intact buffer above the coal-seam roof. The proposed damage-front distance can serve as a numerical screening index before field calibration.

This study has several limits. The two-dimensional plane-strain model is a controlled comparative model and cannot fully represent the three-dimensional nature of borehole blasting. It does not reproduce radial crack networks around a finite borehole, burden-direction breakage, free-surface relief, axial gas leakage, stemming plug movement, or interactions among multiple boreholes. Plane strain may overestimate

confinement and may shift the apparent damage-front position. The material parameters and damage thresholds therefore support relative comparison, not direct prediction of coal loss. The comparison state near 1.0 ms is selected for cross-case model integrity and should not be described as a final fragmentation state. For the decked near-seam cases, late-time stress histories can be influenced by local element erosion around the lower charge; the stress-history discussion is therefore limited to the early vertical stress transfer that supports the damage-front comparison. Field-calibrated three-dimensional work on bottom stemming length, lower charge length, inert interdeck length, air-decking, and multi-hole layouts is needed before the index can be used for design.

4 Conclusions

1. Direct coal-seam damage was not detected at the comparison state, so coal damage depth and width could not distinguish the near-seam cases. The damage-front distance was introduced to measure the remaining intact rock buffer above the seam. This metric captured differences in charge-structure response that were not visible from coal damage depth alone.

2. The coal-side effect of inert-stemming decked charging was boundary dependent. Under the 1.0 m cover condition, the lower damage zone in A4-1.0 approached the coal-seam roof more closely than in A2-1.0. Under the 0.5 m cover condition, A4-0.5 retained a larger intact buffer than A2-0.5. Decked charging should therefore be evaluated together with lower charge position, interdeck location, and remaining rock cover.

3. The coal-rock interface affected stress transfer and damage-front redistribution. The σ_{yy} histories provide mechanism evidence together with the damage maps. Their compressive peaks and C_0/R_0 ratios indicate attenuated vertical transfer from the rock-cover zone to the coal-side monitoring point.

4. The proposed damage-front distance can support pre-design screening of near-seam blasting layouts within a controlled numerical framework. It should not be used as a direct field design criterion before calibration with drilling records, exposed roof conditions, coal loss, dilution, monitoring data, and three-dimensional modelling evidence.

References

1. Zhu, W.C.; Wei, C.H.; Li, S.; Wei, J.; Zhang, M.S. Numerical modeling on destress blasting in coal seam for enhancing gas drainage. International Journal of Rock Mechanics and Mining Sciences 2013. DOI: https://doi.org/10.1016/j.ijrmms.2012.11.004
2. Gao, K.; Huang, P.; Liu, Z.; Liu, J.; Shu, C.; Qiao, G. Coal-rock damage characteristics caused by blasting within a reverse fault and its resultant effects on coal and gas outburst. Scientific Reports 2021. DOI: https://doi.org/10.1038/s41598-021-98581-w

3. Zhu, F.; Liu, Z.; Zuo, Y.; Yang, N.; Huang, A.-C. Damage and failure characteristics of coal and surrounding rock under shaped blasting. Process Safety and Environmental Protection 2023. DOI: https://doi.org/10.1016/j.psep.2023.06.014
4. Liao, Z.; Ding, X.; Liang, M.; et al. Research on the optimization of optimal blasting parameters and fragmentation control based on coal seam geological conditions. Scientific Reports 2025. DOI: https://doi.org/10.1038/s41598-025-94278-6
5. Ding, X.; Lu, X.; Zhou, W.; Shi, X.; Luan, B.; Li, M. Blasting impact simulation test and fragmentation distribution characteristics in an open-pit mine. Shock and Vibration 2019. DOI: https://doi.org/10.1155/2019/4080274
6. Wang, M.; Li, X.; Li, Q.; Hu, Y.; Chen, Q.; Jiang, S. Study on blasting technology for open-pit layering of complex mine adjacent to high and steep slope. Frontiers in Earth Science 2021. DOI: https://doi.org/10.3389/feart.2021.773872
7. Kutter, H.K.; Fairhurst, C. On the fracture process in blasting. International Journal of Rock Mechanics and Mining Sciences & Geomechanics Abstracts 1971. DOI: https://doi.org/10.1016/0148-9062(71)90018-0
8. Ma, G.W.; An, X.M. Numerical simulation of blasting-induced rock fractures. International Journal of Rock Mechanics and Mining Sciences 2008. DOI: https://doi.org/10.1016/j.ijrmms.2007.12.002
9. Meng, N.; Bai, J.; Chen, Y.; Wang, X.; Wu, W.; Wu, B.; Liu, S. Damage evolution mechanisms of rock induced by blasting with the aid of empty-hole effect. Energies 2020, 13, 756. DOI: https://doi.org/10.3390/en13030756
10. Lu, Y.; Jin, C.; Wang, Q.; Han, T.; Zhang, J.; Chen, L. Numerical study on spatial distribution of blast-induced damage zone in open-pit slope. International Journal of Rock Mechanics and Mining Sciences 2023. DOI: https://doi.org/10.1016/j.ijrmms.2023.105328
11. Jhanwar, J.C. Theory and practice of air-deck blasting in mines and surface excavations: a review. Geotechnical and Geological Engineering 2011. DOI: https://doi.org/10.1007/s10706-011-9425-x
12. Ding, C.; Yang, R.; Zhu, X.; Feng, C.; Zhou, J. Rock fracture mechanism of air-deck charge blasting considering the action effect of blasting gas. Tunnelling and Underground Space Technology 2023. DOI: https://doi.org/10.1016/j.tust.2023.105420
13. Ding, C.; Yang, R.; Chen, C.; Zhu, X.; Feng, C.; Xie, Q. Space-time effect of blasting stress wave and blasting gas on rock fracture based on a cavity charge structure. International Journal of Rock Mechanics and Mining Sciences 2022. DOI: https://doi.org/10.1016/j.ijrmms.2022.105238
14. Wei, X.; Li, Q.; Ma, C.; Dong, L.; Zheng, J.; Huang, X. Experimental investigations of direct measurement of borehole wall pressure under decoupling charge. Tunnelling and Underground Space Technology 2022. DOI: https://doi.org/10.1016/j.tust.2021.104280
15. Lou, X.; Zhou, P.; Yu, J.; Sun, M. Analysis on the impact pressure on blast hole wall with radial air-decked charge based on shock tube theory. Soil Dynamics and Earthquake Engineering 2020. DOI: https://doi.org/10.1016/j.soildyn.2019.105905
16. Gao, F.; Tang, L.; Yang, C.; et al. Blasting-induced rock damage control in a soft broken roadway excavation using an air deck at the blasthole bottom. Bulletin of Engineering Geology and the Environment 2023. DOI: https://doi.org/10.1007/s10064-023-03087-6
17. Li, X.; Liu, K.; Sha, Y.; et al. Numerical investigation on blast-induced rock fragmentation with different stemming structures. Geomechanics and Geophysics for Geo-Energy and Geo-Resources 2023. DOI: https://doi.org/10.1007/s40948-023-00654-9
18. Hong, Z.; Tao, M.; Feng, S.; et al. Experimental study of the impact of deck-charge structure on blast-induced fragmentation. Geomechanics and Geophysics for Geo-Energy and Geo-Resources 2025. DOI: https://doi.org/10.1007/s40948-024-00915-1

19. Ding, X.; Yang, Y.; Zhou, W.; et al. The law of blast stress wave propagation and fracture development in soft and hard composite rock. Scientific Reports 2022. DOI: https://doi.org/10.1038/s41598-022-22109-z
20. Cui, J.; Xie, L.; Qiao, W.; et al. Study on blasting characteristics of rock mass with weak interlayer based on energy field. Scientific Reports 2022. DOI: https://doi.org/10.1038/s41598-022-17028-y
21. Fan, L.F.; Shi, X.Y.; Wang, M.; Jiang, F. Wave transmission in layered composite rock mass comprising parallel joints and different rock materials. International Journal of Rock Mechanics and Mining Sciences 2024. DOI: https://doi.org/10.1016/j.ijrmms.2024.105858
22. Li, J.; Ma, G. Analysis of blast wave interaction with a rock joint. Rock Mechanics and Rock Engineering 2010. DOI: https://doi.org/10.1007/s00603-009-0062-0
23. Li, F.; Wang, G.; Xiang, G.; Tang, J.; Ren, B.; Chen, Z. Vibration response of the interfaces in multi-layer combined coal and rock mass under impact load. Processes 2023. DOI: https://doi.org/10.3390/pr11020306
24. Johnson, G.R.; Holmquist, T.J. An improved computational constitutive model for brittle materials. AIP Conference Proceedings 1994. DOI: https://doi.org/10.1063/1.46199
25. Wang, J.; Yin, Y.; Luo, C. Johnson-Holmquist-II (JH-2) constitutive model for rock materials: parameter determination and application in tunnel smooth blasting. Applied Sciences 2018. DOI: https://doi.org/10.3390/app8091675
26. Wang, Z.; Wang, H.; Wang, J.; Tian, N. Finite element analyses of constitutive models performance in the simulation of blast-induced rock cracks. Computers and Geotechnics 2021. DOI: https://doi.org/10.1016/j.compgeo.2021.104172

Open Access This chapter is licensed under the terms of the Creative Commons Attribution-NonCommercial 4.0 International License (http://creativecommons.org/licenses/by-nc/4.0/), which permits any noncommercial use, sharing, adaptation, distribution and reproduction in any medium or format, as long as you give appropriate credit to the original author(s) and the source, provide a link to the Creative Commons license and indicate if changes were made.

The images or other third party material in this chapter are included in the chapter's Creative Commons license, unless indicated otherwise in a credit line to the material. If material is not included in the chapter's Creative Commons license and your intended use is not permitted by statutory regulation or exceeds the permitted use, you will need to obtain permission directly from the copyright holder.

